ELSEVIER

Journal of Alloys and Compounds 330–332 (2002) 250–255

Journal of ALLOYS AND COMPOUNDS

www.elsevier.com/locate/jallcom

Influence of the martensitic transformation on the hydrogenation properties of $Ti_{50-x}Zr_xNi_{50}$ alloys

F. Cuevas[a,*], M. Latroche[a], P. Ochin[b], A. Dezellus[b], J.F. Fernández[c], C. Sánchez[c], A. Percheron-Guégan[a]

[a]*Laboratoire de Chimie Métallurgique des Terres Rares, ISCSA-CNRS, 2–8 rue Henri Dunant, 94320 Thiais Cedex, France*
[b]*Centre d'Études de Chimie Métallurgique, ISCSA-CNRS, 15 rue G. Urbain, 94400 Vitry sur Seine, France*
[c]*Dpto. Física de Materiales, C-IV, Universidad Autónoma de Madrid, Cantoblanco 28049, Madrid, Spain*

Abstract

$Ti_{50-x}Zr_xNi_{50}$ alloys with $0 \leq x \leq 24$ develop either austenitic or martensitic crystal structures when prepared by melt-spinning or induction melting, respectively. This outcome is a consequence of the particular alloy microstructure resulting from each preparation method, which induces a difference of 100°C on the martensitic transformation temperatures for alloys with the same composition. Austenitic alloys absorb hydrogen up to 1.5 hydrogen atoms per AB unit (H/AB) at 130°C and 20 bar, without displaying any plateau pressure for hydrogen pressures between 0.1 and 10 bar. In contrast, martensitic alloys exhibit a plateau pressure with hydrogen concentrations between 1 and 2.1 H/AB, and reach a maximum hydrogen concentration of 2.6 H/AB under the same thermodynamic conditions. Consequently, martensitic alloys form a dihydride compound that, for the representative case of $Ti_{32}Zr_{18}Ni_{50}$ alloy, has a formation enthalpy of -12.3 ± 0.2 kcal mol H_2^{-1}.

Keywords: TiNi; Martensite transformation; Hydrides; Ni–MH batteries

1. Introduction

TiNi is an outstanding alloy because of its shape memory behaviour [1] and hydrogen storage capability [2]. The memory behaviour of TiNi is related to a structural martensitic transformation (MT) from a high-temperature $Pm\bar{3}m$ (B2) cubic structure to a low-temperature $P2_1/m$ (B19′) monoclinic structure. The transformation occurs around 40°C for equiatomic stoichiometry, though its exact value strongly depends on the thermal and mechanical history of the alloy [3,4].

Austenitic TiNi alloy is a valuable material to be used as a negative electrode in MH-batteries [5–8]. It shows good resistance to corrosion in alkaline media, and does not easily decrepitate, but its reversible capacity is limited to one hydrogen atom per AB unit (i.e. 250 mAh/g in equivalent electrochemical units). On the contrary, there are very few available data on the hydrogenation properties of martensitic TiNi alloy. As this phase occurs below room temperature (RT), its hydrogenation is complicated by problems of activation and slow kinetics. However, partial substitution of Ti by Zr has been recently reported to increase the MT temperatures [9], which allows studying the hydrogenation properties of martensitic (Ti,Zr)Ni alloys above RT.

2. Experimental

Alloys with nominal composition $Ti_{50-x}Zr_xNi_{50}$, where x equals 0, 6, 12, 18 and 24 at%, have been prepared in the form of buttons and ribbons by induction melting and melt-spinning, respectively. Massive buttons, namely as-cast alloys, with typical masses of 10 g, were produced by conventional induction melting in a water-cooled copper device starting from the pure elements. To get the desired alloy composition, Ni, Ti and Zr, with nominal purities of 99.9%, were counterbalanced with a precision of 0.1%. The buttons were remelted five times under secondary vacuum and turned over between each melting to ensure their homogeneity. In all cases, mass loss of material during the preparation was lower than 0.01%. As-cast alloys were not annealed after their preparation in order to

*Corresponding author.
E-mail address: fermin.cuevas@glvt-cnrs.fr (F. Cuevas).

0925-8388/02/$ – see front matter
PII: S0925-8388(01)01636-X

avoid, as much as possible, the likely segregation of secondary phases [1]. On the other hand, ribbons of about 40 μm in thickness, denoted as melt-spun alloys, were produced by melt-spinning under helium atmosphere over a stainless-steel wheel having a surface velocity of 19 m/s. In this case, the ingots for melt injection were prepared as described for as-cast alloys followed by liquid solidification over a cylindrical water-cooled copper crucible.

The microstructure and composition of the alloys were analysed after mechanical polishing by electron microscopy and electron probe microanalysis (EPMA) in a Cameca SX-100 EPMA instrument operated at 20 kV. Their crystal structures at RT were studied by X-ray diffraction (XRD) using Cu Kα radiation in a Bruker AXS D8Advance θ–θ diffractometer. Differential scanning calorimetry (DSC) was used to determine MT temperatures of the alloys in a DSC-4 Perkin-Elmer calorimeter operated at a heating/cooling rate of 10°C/min. Finally, their hydrogenation properties were studied by solid-gas reaction in a Sievert's type apparatus to get their Pressure–Composition–Isotherm (PCI) curves. Prior to hydrogenation, samples were etched with 10% HF solution for 30 s to eliminate superficial oxides.

3. Results and discussion

3.1. Alloy characterisation

The chemical compositions of the prepared alloys are given in Table 1. Both as-cast and melt-spun alloys have chemical compositions close to the nominal values with a Ni content slightly lower than 50 at%. This deviation induces a small amount of $(Ti,Zr)_2Ni$ precipitation which, as observed by optical metallography, extends over a volume fraction lower than 3%. Considering the characteristics of the binary Ti–Ni diagram [10] and the EMPA results, the composition of the major phase is estimated to be $(Ti,Zr)_{50.5}Ni_{49.5}$. Additionally, backscattered electron micrographs and EMPA analyses show that as-cast alloys exhibit notable compositional fluctuations in the micron range between Zr and Ti concentrations (Fig. 1a). These fluctuations are not observed for melt-spun alloys (Fig. 1b) which, however, present extended superficial defects, mainly voids and scratches, related to the melt-spinning technique.

XRD measurements at RT reveal distinct crystal structures for the major (Ti,Zr)Ni phase in as-cast and melt-spun alloys (Fig. 2). In the former state, the alloys exhibit the monoclinic martensitic phase (B19′) with space group $P2_1/m$, whereas in the latter, materials have a cubic austenitic phase (B2) with CsCl-type structure. A linear increment of the unit cell volume with the Zr-content is observed in both crystallographic structures (Table 1) due to the higher atomic radius of Zr (1.60 Å) with respect to Ti (1.47 Å). Concerning as-cast alloys, the large peak broadening in their XRD patterns seems to be mainly related to the martensitic transformation, though the mentioned local fluctuations between Ti and Zr must also contribute to this effect. A more detailed structural analysis of these alloys is reported elsewhere [11].

The different crystal structures exhibited by as-cast and melt-spun alloys at RT can be well understood in terms of their distinct MT temperatures. As displayed in Fig. 3 for the representative case of $x=6$, DSC measurements show that, on cooling, the martensitic transformation proceeds in melt-spun alloys at temperatures about 100°C lower than those in as-cast alloys. This permits the MT to occur above and below RT in as-cast and melt-spun alloys, respectively. By comparison with the induction technique, the high quenching rates achieved by melt-spinning causes hindering of the martensitic phase growth in melt-spun alloys. Such stabilisation of austenite is commonly ascribed in the literature either to a reduction of grain size or to the occurrence of fine precipitates [12,13].

3.2. Hydrogenation properties

In order to get fast kinetics for hydrogen absorption and to avoid activation problems, PCI curves were measured at 130°C. However, the martensitic crystal structure can be transformed to austenite while heating. Therefore, the reverse MT temperatures (i.e. those corresponding to the austenite formation on heating) were investigated by DSC in as-cast alloys. It is worth noting that heating cannot transform the austenitic structure of melt-spun alloys. The reverse transformation start, A_s, and finish, A_f, temperatures were determined by the tangential extrapolation

Table 1
Chemical composition and cell volume per AB of the alloys prepared in this investigation

x (at%)	As-cast alloys		Melt-spun alloys	
	Composition (at%)	Cell volume (Å^3/AB)	Composition (at%)	Cell volume (Å^3/AB)
0	$Ti_{50.8\pm0.4}Ni_{49.2\pm0.4}$	27.53(2)	$Ti_{51.0\pm0.1}Ni_{49.0\pm0.1}$	27.43(1)
6	$Ti_{44.7\pm1.5}Zr_{6.5\pm1.5}Ni_{48.8\pm0.4}$	28.16(1)	$Ti_{44.9\pm0.1}Zr_{5.9\pm0.1}Ni_{49.2\pm0.1}$	28.01(2)
12	$Ti_{38.6\pm1.2}Zr_{12.4\pm1.2}Ni_{49.0\pm0.6}$	28.94(2)	$Ti_{38.9\pm0.1}Zr_{11.7\pm0.1}Ni_{49.4\pm0.1}$	28.65(1)
18	$Ti_{32.6\pm1.1}Zr_{18.1\pm1.2}Ni_{49.2\pm0.5}$	29.87(2)	$Ti_{32.8\pm0.1}Zr_{17.5\pm0.1}Ni_{49.7\pm0.1}$	29.27(1)
24	$Ti_{26.4\pm0.5}Zr_{24.3\pm0.7}Ni_{49.3\pm0.7}$	30.58(3)	$Ti_{26.9\pm0.1}Zr_{23.6\pm0.1}Ni_{49.5\pm0.1}$	29.93(2)

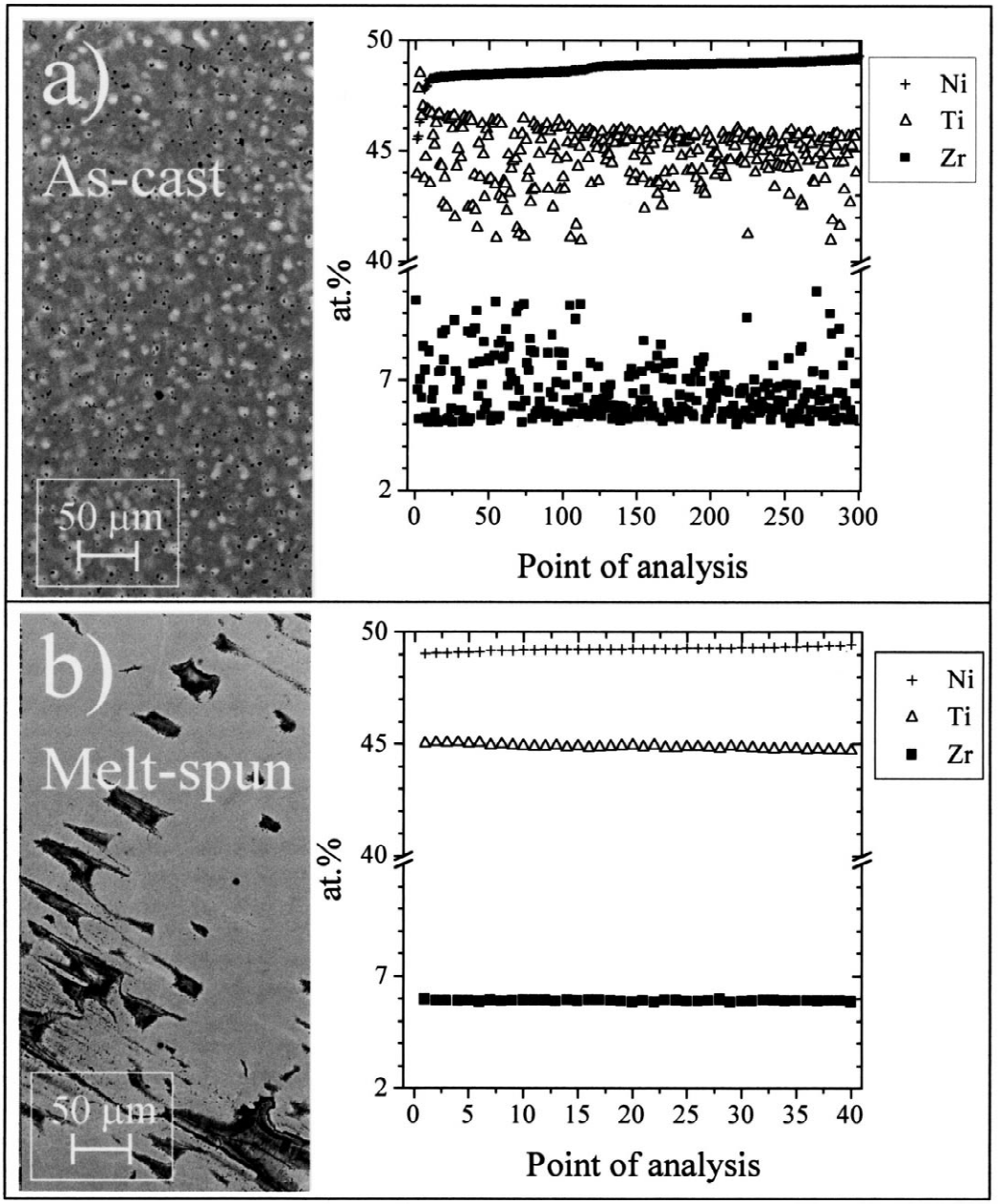

Fig. 1. Backscattered electron micrographs and EMPA analysis of as-cast (a) and melt-spun (b) alloys for the representative case of $x=6$.

method [14] and are displayed together with the peak temperature, A_p, in Fig. 4 and Table 2. In agreement with previous results of Hsieh and Wu [9], Zr-substitution stabilises the martensite, especially for Zr contents higher than 18 at%. At 130°C, as-cast alloys are fully austenite for $x=0$ but fully martensite for $x=24$. Both phases coexist at 130°C for intermediate Zr contents, though A_p values suggest that austenite is mainly present at low Zr contents ($x=6$ and 12) while martensite mostly occurs at high Zr contents ($x=18$). It is also worth remarking that the interval of transformation temperature, $A_f - A_s$, suddenly increases with the incorporation of zirconium to the TiNi alloy, which is likely related to the mentioned local fluctuations between Zr and Ti.

PCI curves at 130°C were conducted in both melt-spun and as-cast alloys for hydrogen equilibrium pressures, P_{H_2}, within the range 0.1–20 bar, and are displayed in Figs. 5 and 6, respectively. It has been observed that all alloys absorb hydrogen instantaneously at about 10 bar. As a further common feature, they present a rather stable hydrogen absorption for $0<y<1$ (where y denotes the ratio H/AB) since P_{H_2} is lower than 0.1 bar within this concentration region. The particular PCI characteristics for each alloy type is described in the following.

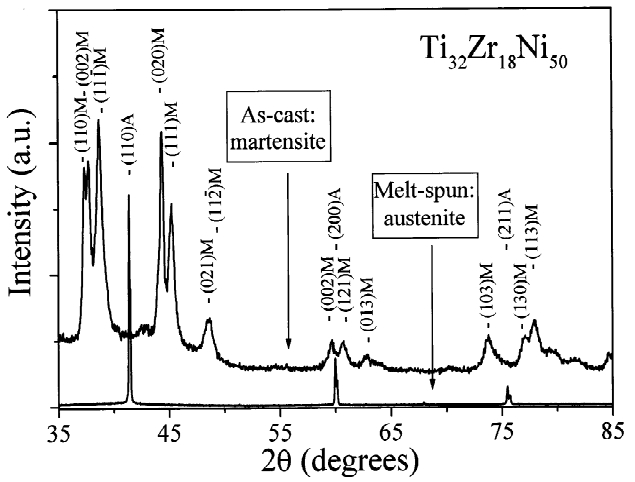

Fig. 2. XRD patterns at R.T. of as-cast and melt-spun alloys with $x=18$.

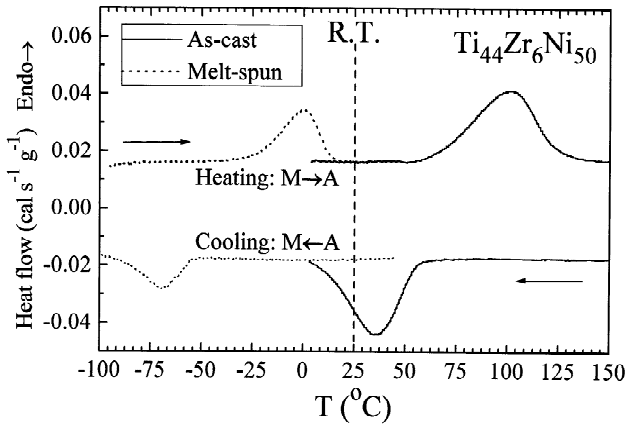

Fig. 3. DSC scans from as-cast and melt-spun alloys with $x=6$ measured at a cooling and a heating rate of 10°C/min.

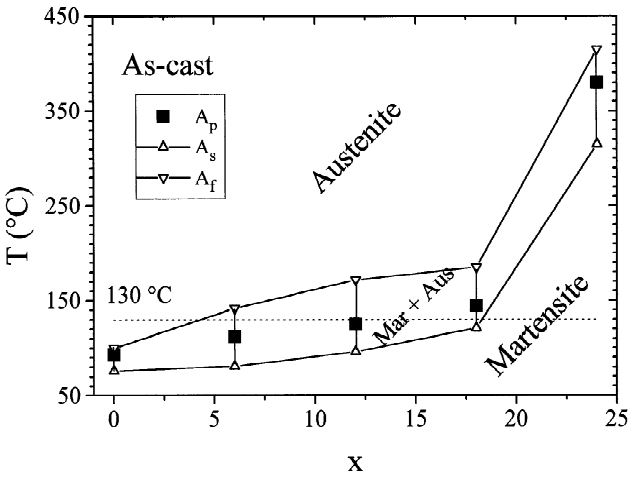

Fig. 4. Reverse martensitic transformation temperatures and domain phases in as-cast $Ti_{50-x}Zr_xNi_{50}$ alloys obtained from DSC measurements.

Table 2
Reverse MT temperatures in as-cast $Ti_{50-x}Zr_xNi_{50}$ alloys obtained from DSC measurements

x (at%)	A_s (°C)	A_p (°C)	A_f (°C)	$A_f - A_s$ (°C)
0	76±1	93±1	100±1	24±1
6	81±2	112±2	142±2	61±2
12	96±3	125±3	172±3	76±3
18	121±2	144±2	185±2	64±2
24	320±15	380±15	415±15	95±15

A_s stands for the start of austenite formation; A_f is the finish of austenite formation, and A_p is the transformation peak temperature.

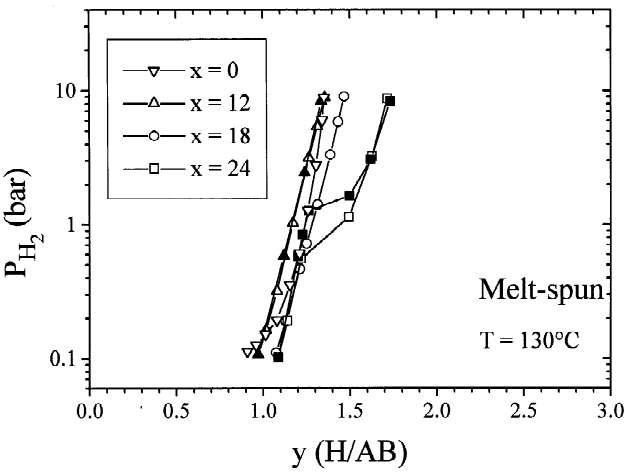

Fig. 5. PCI-curves at 130°C of melt-spun $Ti_{50-x}Zr_xNi_{50}$ alloys. Full symbols correspond to absorption and empty symbols to desorption.

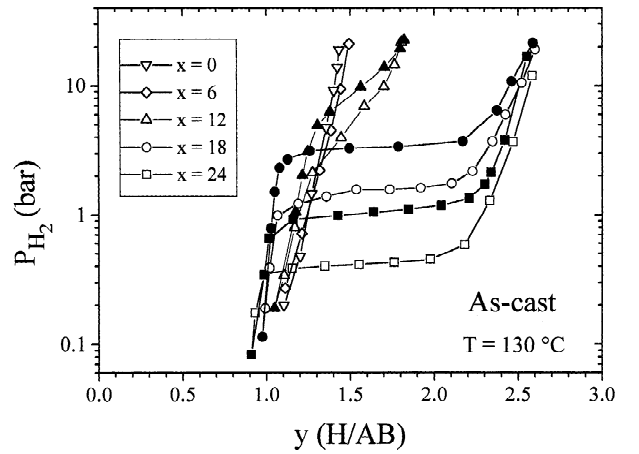

Fig. 6. PCI-curves at 130°C of as-cast $Ti_{50-x}Zr_xNi_{50}$ alloys. Full symbols correspond to absorption and empty symbols to desorption.

The isotherms for melt-spun austenitic alloys (Fig. 5) exhibit for $x<24$ no invariant plateau pressure, which indicates a solid solution of hydrogen in the alloy. Consequently, their hydrogen content gradually varies between $y=1$ at $P_{H_2}=0.1$ bar and $y=1.5$ at $P_{H_2}=10$ bar. No

hysteresis phenomenon is observed upon hydrogen absorption/desorption. A similar hydrogenation behaviour has been described by Burch and Mason in austenitic TiNi [2]. Thus, it can be concluded that moderate Zr-substitution in melt-spun alloys does affect significantly the hydrogenation properties of austenitic TiNi. However, for $x=24$, a short plateau pressure appears at about 1 bar which is most likely related to the presence of a small amount of residual martensite, and contrast with the PCI characteristics of as-cast alloys in which a significant plateau pressure is observed for $x \geq 18$. From Fig. 4, this is consistent with the stabilisation of martensite at the higher Zr contents (Fig. 6).

For as-cast alloys at low Zr-contents ($x=0$ and 6), similar PCI curves as for melt-spun alloys are obtained as a result of their common austenitic structure. On the other hand, when martensitic alloys are hydrogenated (i.e. for high Zr-contents ($x=18$ and 24)) a wide plateau pressure emerges with hydrogen concentration extending from $y=1.0$ to $y=2.1$. A maximum hydrogen content of $y=2.6$ is finally attained at $P_{H_2}=20$ bar. The observed plateau reveals the formation of a hydride phase which is accompanied by a rather strong hysteresis behaviour. For instance, plateau absorption occurs at $P_{H_2}=3.3$ bar while desorption takes place at $P_{H_2}=1.6$ bar for $x=18$. The plateau pressures decrease with the Zr-content, as expected from the increment of the cell volume (Table 1) and Lundin's geometrical model [15]. Eventually, for intermediate Zr-contents ($x=12$), a mixed behaviour occurs with a short sloping plateau, which points towards a transition stage between the hydrogenation properties of low and high Zr-substituted as-cast alloys. This transition can be easily understood in the light of the reversal MT temperatures determined by DSC (Fig. 4). The as-cast alloys remaining as martensite on heating at 130°C, i.e. those with $x>12$, are able to form a novel hydride compound in contrast to austenitic alloys. The composition of this hydride is (Ti,Zr)NiH_y ($y\sim2.1$).

The thermodynamics of the novel hydride have been characterised for martensite $Ti_{32}Zr_{18}Ti_{50}$ by obtaining Van't Hoff plots from absorption and desorption PCI curves within the range 70–130°C (Fig. 7). The isotherms present a slightly sloping plateau due to a minor austenite segregation. The formation entropy of the hydride is about -32 cal K^{-1} mol H_2^{-1} in agreement with standard values of hydride formation due to the transformation of one mole of hydrogen gas into two solid-state protons. The formation enthalpy is -12.3 ± 0.2 kcal mol H_2^{-1}, which is placed between those reported for the monohydride of the well-known hydrogen storage compound TiFe, $\Delta H_f^o=-6.7$

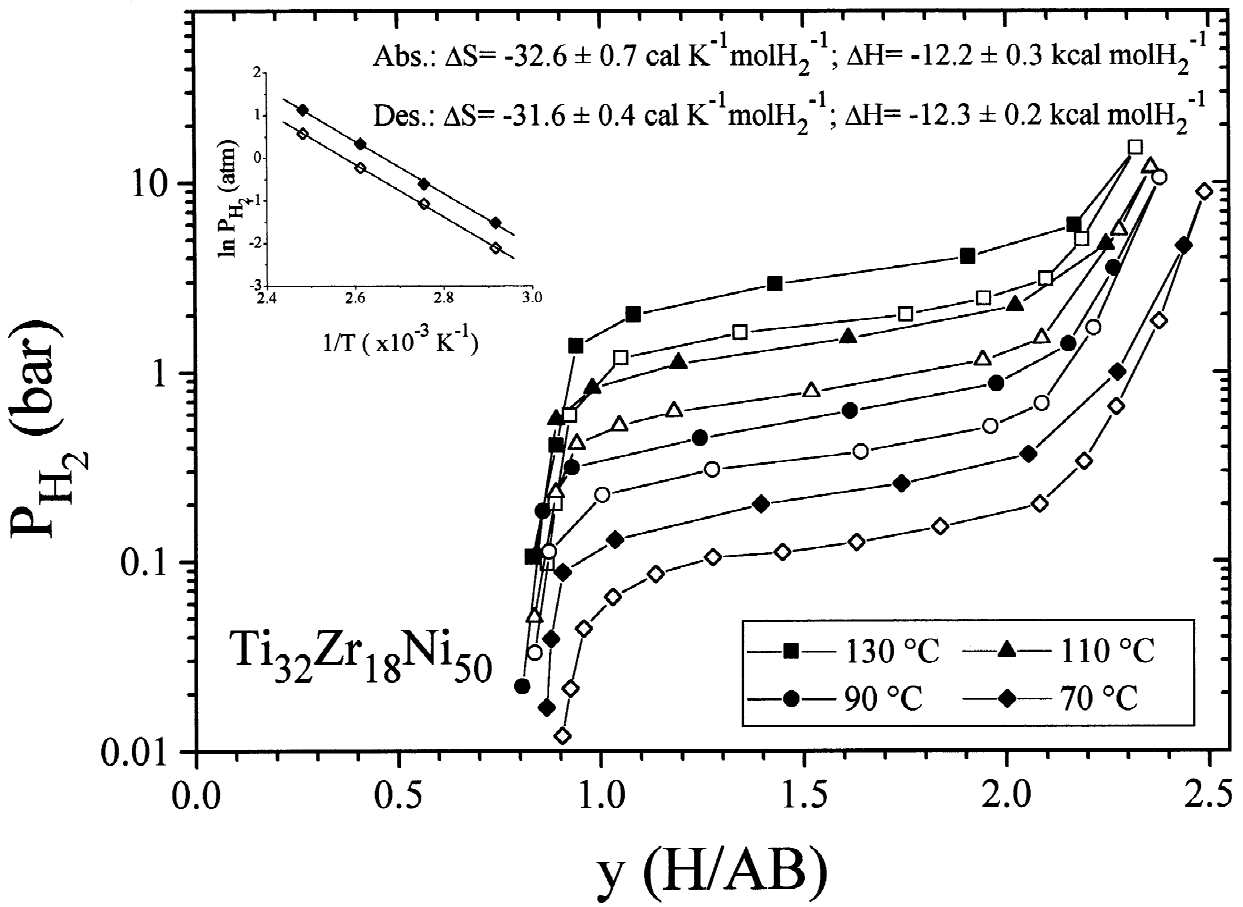

Fig. 7. PCI-curves of martensitic $Ti_{32}Zr_{18}Ni_{50}$ alloy and related Van't Hoff plots. Full symbols correspond to absorption and empty symbols to desorption.

kcal mol H_2^{-1} [16], and the hydride $TiNiH_{0.9}$ obtained from austenitic TiNi, $\Delta H_f^o = -14.3$ kcal mol H_2^{-1} [2].

The main interest of the hydride formation in martensitic TiNi-alloys is hydrogen storage and battery applications. Concerning the latter, PCI curves indicate that the maximum hydrogen capacity in these alloys, when expressed in electrochemical units, is about 550 mAh/g. In contrast, the capacity of austenitic TiNi alloy is only 250 mAh/g. Furthermore, preliminary experiments with a martensitic $Ti_{32}Zr_{18}Ti_{50}$ alloy exhibit a discharge capacity as high as 335 mAh/g at a kinetic regime of C/10 (where C/10 stands for the discharge of full capacity in 10 h). Wakao et al. already reported that Zr-substituted TiNi electrodes offer improved hydrogen capacities but offered no definitive explanation [17,18]. The precipitation of martensite may account for this result. Finally, it is worth pointing out that martensitic alloys suffer from strong decrepitation upon hydrogenation whereas this is not the case for austenitic alloys. This can induce important variations between the cycle life-time of martensitic and austenitic electrodes, a subject which is now under investigation.

4. Conclusion

$Ti_{50-x}Zr_xNi_{50}$ alloys, with $x = 0$, 6, 12, 18 and 24 at%, can be obtained either as austenite or as martensite when prepared by induction melting or melt-spinning, respectively. For alloys with the same chemical compositions, the distinct cooling rates associated with each preparation method cause different microstructural properties and a subsequent disparity of ~100°C on the alloy martensitic transformation temperatures. Austenitic and martensitic alloys show different hydrogenation properties as revealed by PCI curves at 130°C. Austenitic alloys exhibit no clear plateau pressure and a maximum hydrogen content of 1.5 H/AB at 20 bar. In contrast, martensitic alloys exhibit a wide plateau pressure, reflecting the formation of a hydride phase, and a maximum hydrogen content of 2.6 H/AB at 20 bar. Therefore, the martensitic structure is able to store a much higher amount of hydrogen than the austenitic one, which could be relevant for electrochemical and storage applications.

Acknowledgements

The authors wish to thank F. Briaucourt and E. Leroy for technical assistance. F. Cuevas is grateful to the European Community for financial support.

References

[1] K. Otsuka, X. Ren, Intermetallics 7 (1999) 511.
[2] R. Burch, N.B. Mason, J. Chem. Soc. Faraday Trans. 1 75 (1979) 561.
[3] S. Miyazaki, Y. Igo, K. Otsuka, Acta Metall. 34 (1986) 2045.
[4] Y. Liu, G.S. Tan, Intermetallics 8 (2000) 67.
[5] E.W. Justi, H.H. Ewe, A.W. Kalberlah, N.M. Saridakis, M.H. Schaefer, Energy Convers. 10 (1970) 183.
[6] M.A. Gutjahr, Ph. D. Thesis, Geneva University, 1974 (in French).
[7] K. Machida, M. Enyo, G. Adachi, J. Shiokawa, Electrochim. Acta 29 (1984) 807.
[8] D. Fruchart, J.-L. Soubeyroux, S. Miraglia, S. Obbade, G. Lorthioir, F. Basile, D. Colin, F. Faudot, P. Ochin, A. Dezellus, Z. Phys. Chem. 179 (1993) 225.
[9] S.F. Hsieh, S.K. Wu, J. Alloys Comp. 266 (1998) 276.
[10] J.L. Murray, in: J.L. Murray (Ed.), Phase Diagrams of Binary Titanium Alloys, ASM International, Metals Park, Ohio, 1987, p. 197.
[11] F. Cuevas, M. Latroche, P. Ochin, A. Dezellus, J.F. Fernández, C. Sánchez, A. Percheron-Guégan, Proceedings of the Rencontre Franco-Espagnole sur la chimie et physique de l'état solide, Carcans, France, 2000, p. O32.
[12] Z. Nishiyama, in: M.E. Fine, M. Meshii, C.M. Wayman (Eds.), Martensitic Transformations, Academic Press, New York, 1978, p. 283.
[13] J. Dutkiewicz, T. Czeppe, J. Morgiel, Mater. Sci. Eng. A. 273–275 (1999) 703.
[14] W.A. Johnson, J.A. Domingue, S.H. Reichman, F.E. Sczerzenie, J. de Phys. Proc. ICOMAT-82 43 (Suppl. 12) (1982) 285.
[15] C.E. Lundin, F.E. Lynch, C.B. Magee, J. Less-Common Met. 56 (1977) 19.
[16] J.J. Reilly, R.H. Wiswall, Inorg. Chem. 13 (1974) 218.
[17] S. Wakao, Y. Yonemura, H. Nakano, H. Shimada, J. Less-Common Met. 104 (1984) 365.
[18] S. Wakao, H. Sawa, H. Nakano, S. Chubachi, M. Abe, J. Less-Common Met. 131 (1987) 311.